Inorganic Chemistry
Article
Cite This: Inorg. Chem. 2019, 58, 16250−16255
pubs.acs.org/IC

Regioselective Oxidation of C−H Bonds in Unactivated Alkanes by a Vanadium Superoxo Catalyst Bound to a Supramolecular Host

Mahesh Sundararajan,[†,‡] Bohyun Park,[‡,†] and Mu-Hyun Baik*[,†,‡]

[†]Center for Catalytic Hydrocarbon Functionalizations, Institute for Basic Science (IBS), Daejeon 34141, Republic of Korea
[‡]Department of Chemistry, Korea Advanced Institute of Science and Technology (KAIST), Daejeon 34141, Republic of Korea

Supporting Information

ABSTRACT: A vanadyl ion bound to a cucurbituril (CB) host was reported to oxidize pentane to 2-pentanol in the presence of an oxidizer. DFT calculations suggest that the catalyst selectively reacts with stronger C−H bonds in pentane over weaker C−H bonds in cyclohexane due to size exclusion by the CB host. The active catalyst is an unprecedented vanadium superoxo species bound to the host, and the selectivity toward secondary over the primary C−H bond is the result of a higher degree of charge transfer from the secondary compared to the primary position.

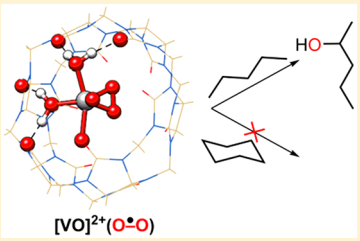

INTRODUCTION

One of the major challenges in chemistry is to understand the structure−function relationship of metalloenzymes in catalyzing reactions with high levels of site-selectivity.[1] Many organometallic catalysts were prepared to mimic metalloenzymes with some success.[2] Supramolecular hosts can mimic the enzymes due to their unique shapes,[3,4] and one of the popular macrocyclic hosts is cucurbituril (CB), a pumpkin-shaped supramolecule.[5] Based on the number of monomer units, the host can accommodate guests of different sizes and shapes.[6] The hydrophilic portals and the hydrophobic core make these hosts special and facilitate the binding of a wide range of molecules.[7] Recently, a vanadyl ion ($[VO]^{2+}$) bound to CB-[6] portals was reported to oxidize pentane to 2-pentanol in the presence of oxidants such as hydrogen peroxide or iodosobenzene (PhIO) solution.[8] The reaction is not clean and side-products are observed, and thus, a radical-based mechanism was proposed.[9] The catalyst encapsulated by the CB is substrate selective and oxidizes only pentane but not cyclohexane, as illustrated in Scheme 1.

Unfortunately, neither the exact structure of the catalyst nor the possible reaction mechanism responsible for the selectivity are known. Based on the UV−vis and EPR spectroscopic data, it was proposed that the $[VO]^{2+}$ binds symmetrically to the CB-[6] host, but a simple inspection of the cage size in comparison to the molecular size of the $[VO]^{2+}$ functionality shows that symmetrical binding is not possible. Little is known about the electronic structures of the catalytically competent species, which may either consist of a high-valent V(V)-peroxo species[10−13] or the corresponding one electron oxidized V(V)-superoxo analogue.[14−17]

To shed light on the reaction mechanism and better understand how such a simple molecular entity is turned into an intriguing supramolecular catalyst, density functional theory (DFT) calculations were carried out. First, the computationally derived geometry and electronic structure of $[VO]^{2+}$ bound to CB-[6] were assessed to identify and characterize the catalytically active species that can promote C−H activation. Next, we investigated why the much stronger C−H bond in pentane[18] is oxidized instead of the weaker C−H bonds in cyclohexane.[19] Finally, we investigated the molecular basis for the experimentally observed regioselectivity in the reaction with pentane.

Scheme 1. Proposed Substrate Selective Supramolecular Catalysis

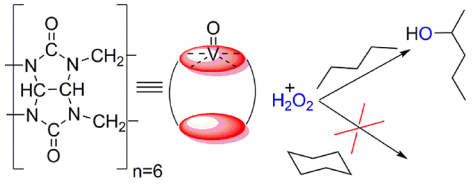

RESULTS AND DISCUSSION

We have explored several geometric structures of vanadyl binding to CB-[6], as shown in Figure S1. First, a C_6-symmetric binding of vanadyl to CB-[6] is considered, and upon geometry optimization, we find that such binding is not plausible due to the larger cavity of CB-[6]. The vanadyl ion can bind only with two CB-[6] carbonyl portals. Second, the oxygen atom of vanadyl can face either inside or outside the CB-[6] cavity. Finally, the uncoordinated vanadyl ion should be saturated with solvent molecules such as water molecules. Thus, after exploring several possibilities, we concluded that the most plausible structure of **1** consists of a square-pyramidal vanadium center placing the oxo moiety in the axial position. Two oxygens of CB-[6] are directly bound to the vanadium,

Received: September 20, 2019
Published: November 13, 2019

DOI: 10.1021/acs.inorgchem.9b02803
Inorg. Chem. 2019, 58, 16250−16255

and the remaining coordination sites are saturated by water molecules that are strongly hydrogen-bonded to the other oxygens of the CB-[6] host, as illustrated in Figure 1. The technical details of the calculations are summarized in the Experimental Section.

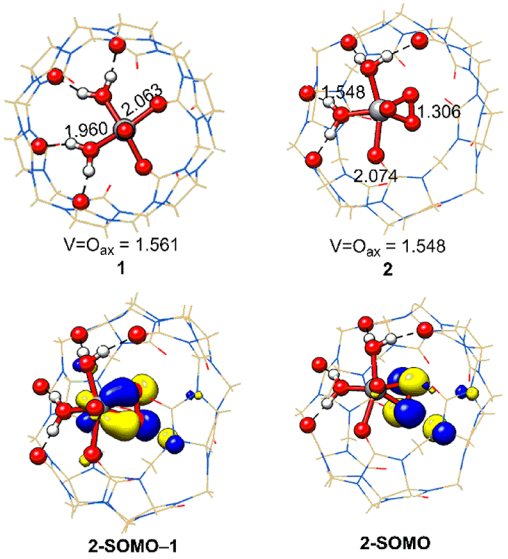

Figure 1. Optimized structures of **1** and **2**. Frontier orbitals showing the superoxo moiety of **2**. Isodensity value = 0.05 au. Units for bond lengths in angstroms (Å).

Table 1 compares the previously determined experimental EPR parameters to calculated values at the proposed geometry of **1**. The calculations are in good agreement with the experimental data. As expected for a V(IV)-d^1 center in pseudosquare-pyramidal coordination geometry, the single valence electron is localized in the nonbonding d_{xy} orbital.[20] The axial type g-tensor that is expected for the $3d^1$ electronic configuration is nicely reproduced by the calculations, and the experimental g-tensors of 1.921 and 1.970 are fairly well-matched with calculated values of 1.952 and 1.985. The unpaired electron on the metal center will have a large ^{51}V hyperfine coupling constant, which is reliably reproduced within 2 MHz with the calculated isotropic coupling constant being 324 MHz compared to the experimentally determined 326 MHz.

Table 1. Computed Spectral Parameters of 1 and 2

	DFT	experiment	DFT	experiment
structure	**1**	**1**	**2**	**2**
g-tensor	1.952, 1.985	1.921, 1.970	2.004, 2.009	2.012[c]
^{V}A (MHz)[a]	212, 218, 542 (324)	213, 221, 546 (326)[b]	2	7[c]

[a]Values in parentheses are the corresponding isotropic values. [b]Ref 8. [c]Ref 17.

When the vanadyl ion bound to CB-[6] is exposed to a hydrogen peroxide solution, the vanadium center is readily oxidized and the high-valent V(V)-oxo-superoxo species denoted as **2** in Figure 1 is formed. Our calculations predicted that one of the equatorial V−O bonds is cleaved to expose a free coordination site where dioxygen binds side-on. This superoxo moiety was very well represented as the computed O−O bond length and the vibrational frequency were 1.31 Å and 1169 cm^{-1}, respectively, in good agreement with experimentally observed bond lengths[21,22] and the vibrational frequency of 1124 cm^{-1}. In **2**, the unpaired electron is dominantly localized on the dioxygen fragment as shown in **2-SOMO**, whereas the unpaired electron was vanadium-centered in **1**. This relocation of the radical character is consistent with the oxidation of the vanadyl moiety and reduction of the dioxygen moiety to a superoxo species. The metal-centered oxidation is also indicated by the negligibly small hyperfine coupling constant, measured[17] to be 7 MHz and calculated to be 2 MHz. The formation of high-valent VO-superoxo species (eq 1) is energetically favorable by 4.3 kcal/mol.

$$\mathbf{1} + 2H_2O_2 \rightarrow \mathbf{2} + 2H_2O \quad (1)$$

High-valent V(V)-peroxo species were frequently observed in the past, but analogous superoxo species are rare,[14−17] which is not surprising given the reactive nature of such radical species. Mayer et al.[12] reported the slow reactivity of V(V)-oxo-peroxo species toward hydrogen atom transfer (HAT), whereas Yin and co-workers[16] reported that V(V)-oxo-superoxo species can be stabilized with non-redox metal ions that can promote HAT.

The CB hosts are known to bind cations and are effective in stabilizing radical species. For instance, the half-life of TEMPO-like nitroxide radicals can be extended to as long as 254 min upon encapsulation to CB-[7].[23] Our calculations suggest that the vanadyl superoxo radical is similarly stabilized inside the CB-[6] cage and that it plays a pivotal role for the C−H activation. To commence the C−H activation reaction, the substrates must enter the host cavity and approach the superoxo moiety through the CB cage. With a portal diameter of 3.9 Å, CB-[6] can act as an effective filter that only allows small substrates to access the reactive superoxo moiety inside the cage.[6,24] Specifically, cyclohexane is 5.2 Å wide and cannot enter the CB-[6] cavity, whereas pentane is small enough at ∼2.0 Å to be able to enter the host as illustrated in Figure 2.

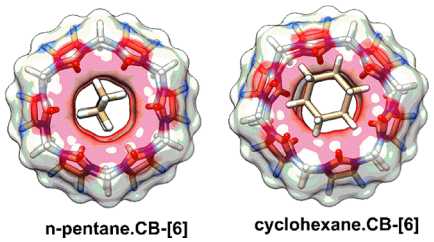

Figure 2. Hydrophobicity surface of CB-[6] showing the restricted entry of cyclohexane over *n*-pentane.

Florea and Nau reported previously that cyclohexane and *n*-hexane do not bind to CB-[6].[25,26] Extensive electronic structure calculations were employed to show that the binding of simple hydrocarbons to CB-[6] is primarily under kinetic control determined by the interaction of the portal with the substrate, which ultimately leads to the substrate selectivity.[26]

Interestingly, the CB complex **2** is not only substrate selective but also regioselective as it activates the C−H bond of pentane (**3**) to give 2-pentanol. As illustrated in Scheme 2 and Figure 3, our calculations showed that the reaction most likely proceeds via the HAT step, followed by the rebound (RB) of the alkyl radical, which is one of the classic mechanisms of C−H activation that is found in many biological systems, such as

DOI: 10.1021/acs.inorgchem.9b02803
Inorg. Chem. 2019, 58, 16250−16255

Scheme 2. Proposed Mechanism for C−H Activation by 2

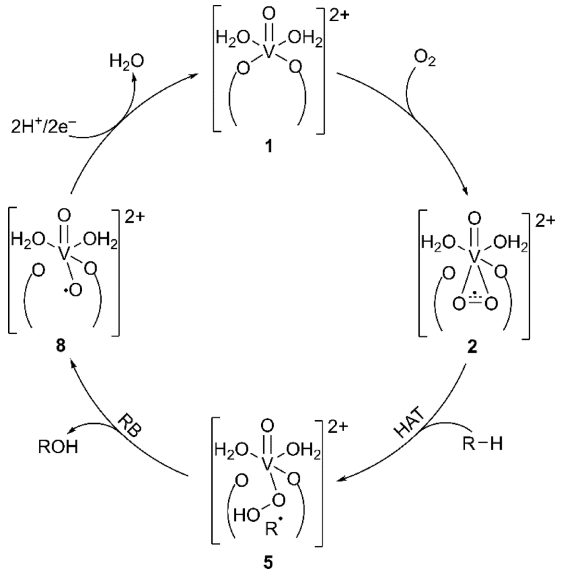

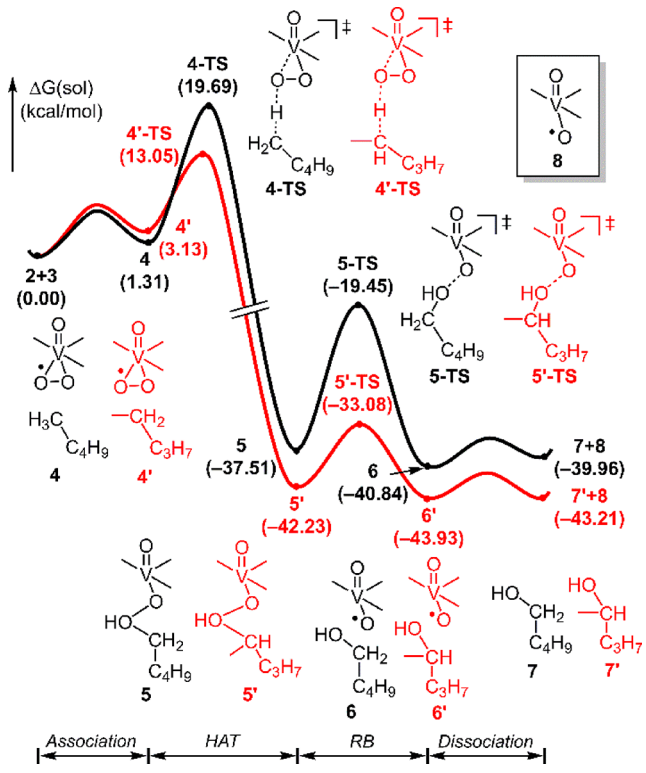

Figure 3. Computed energy profile of **2** with **3**. Black and red traces are toward 1-pentanol and 2-pentanol production, respectively. All species except **3**, **7**, and **7′** have positive two charges.

cytochrome P450-enzymes[27] or methane monooxygenases.[28] The size-based exclusion of cyclohexane is not a surprising finding, but the observed selectivity toward the secondary carbon is puzzling. As the CB-framework mimics an enzymatic pocket for the V-superoxo fragment, it is easy to envision that the linear pentane substrate enters the reaction site in a linearly stretched fashion, which should bring the terminal, primary C−H bond into a preferred, most immediate contact. It is curious therefore that 2-pentanol is the main product. Interestingly, our DFT calculations reproduce this observed selectivity reliably, indicating that there are effects at play that go beyond using the CB-scaffold to control the reactant binding geometry.

The energy profiles for the full reaction mechanism shown in Figure 3 illustrate that HAT from the secondary C−H bond traversing **4′-TS** requires only 13.1 kcal/mol. In contrast, the analogous of the primary C−H bond is associated with a barrier of 19.7 kcal/mol. This energy difference of the two transition states is notably larger than the difference in the free bond dissociation energies of 101.6 versus 98.5 kcal/mol for the primary and secondary C−H bonds of pentane.[18] Unsurprisingly, the entropy and solvation energy changes are very similar for both **4-TS** and **4′-TS**, so it is the electronic energy difference that determines the overall preference of **4′-TS**. To understand the origin of this surprisingly large regioselectivity, two transition states, **4-TS** and **4′-TS**, were fragmentized into pentane substrate and CB fragments and their distortion-interaction energies[29] were analyzed as summarized in Figure 4.

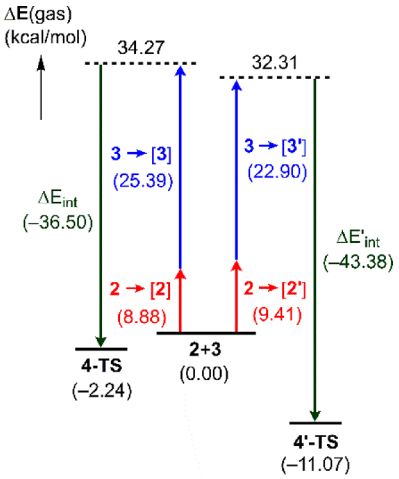

Figure 4. Fragment energy decomposition analysis of **4-TS** and **4′-TS**.

In this analysis the reactants **2** and **3** are first distorted into the structures that they adopt in the transition states, marked as [**2**], [**2′**], [**3**], and [**3′**], and are then allowed to interact with each other. The structural distortion energies of **2** → [**2**] and **2** → [**2′**] were similar at +8.9 and +9.4 kcal/mol, respectively. Meanwhile, the superoxo functionality becomes significantly reduced at the transition state with the O−O bond length increasing notably from 1.31 Å in **2** to 1.40 and 1.41 Å in **4-TS** and **4′-TS**, respectively. This structural change is associated with energy penalties of 25.4 and 22.9 kcal/mol to result in similar total distortion energies of 34.3 and 32.3 kcal/mol, respectively. However, the total electronic energy is 8.8 kcal/mol more preferable in **4′-TS** because in **4-TS** the electronic interaction between [**2**] and [**3**] gives −36.5 kcal/mol, whereas much stronger interaction of −43.4 kcal/mol is found in **4′-TS**. These energies indicate that the main cause of the regioselectivity lies in the electronic changes that take place at the transition state,[29] rather than due to any structural differences. A more detailed inspection of the calculations reveals that the net charge transferred from the substrate to the superoxo moiety of the catalyst are 0.20 e^- and 0.33 e^-, respectively. This charge transfer trend is easy to understand as the more substituted secondary carbon center can tolerate a

DOI: 10.1021/acs.inorgchem.9b02803
Inorg. Chem. 2019, 58, 16250−16255

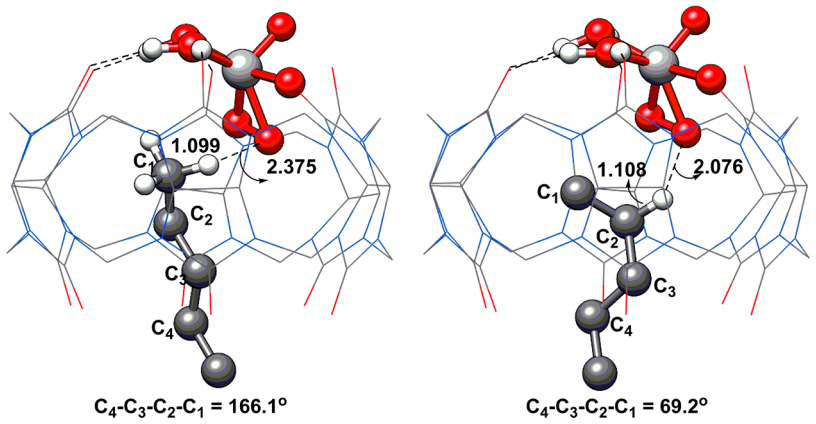

Figure 5. Associative binding of pentane to **2** to form **4** and **4′**. Units in angstroms (Å). Unnecessary hydrogen atoms are omitted for clarity.

higher positive charge than the primary analogue. As a consequence, the superoxo fragment shows a higher extent of peroxo character, which is energetically favorable. Furthermore, CB portals are known to stabilize positive species over neutral and anionic species through favorable ion-dipole interactions.[30−32] Thus, the higher induced positive charges of the pentane present in **4′-TS** will be more stabilized by CB-[6] portals than those of **4-TS**. In Figure S2, the electrostatic potential maps of the two transition states are shown to illustrate this feature.

Once the intermediates **5** and **5′** at −33.1 and −42.2 kcal/mol, respectively, are formed, O−O bond cleavage ensues via **5-TS** and **5′-TS** to afford the final products 1- and 2-pentanol with the step barriers of 18.1 and 9.1 kcal/mol, respectively. The much lower barrier associated with **5′-TS** is the result of strong hydrogen bonds between the hydroxo group and the CB-[6] wall (Figure S3), which is not present in **5-TS**. Dissociation of the products from the intermediates **6** and **6′** is easy, and the primary and secondary alcohols **7** and **7′** dissociate from the host, leaving behind a vanadium oxo-oxyl species, **8**, bound to CB-[6]. Species **8** can regenerate the resting state **1** through the addition of two protons and two electrons.

For understanding the aforementioned structural preference toward the terminal over the secondary position in the CB-binding pocket, it is instructive to inspect the intermediates **4** and **4′** in greater detail. The main difference between these two intermediates is the orientation of the substrate in the binding pocket. In **4** the primary carbon points toward the superoxo moiety, whereas the secondary carbon of pentane is oriented toward it in **4′**, as shown in Figure 5. Interestingly, the secondary C−H bond in **4′** is positioned at a hydrogen−oxygen distance of 2.08 Å, which is 0.3 Å closer than where the primary C−H bond is found in **4**. Furthermore, the dihedral angles of pentane in **4** and **4′** are very different at 166.1° and 69.2°, respectively. Such dihedral rotations are the early stage hydrocarbon coiling as extensively studied by Rebek Jr. in constrained macrocyclic containers.[33] Similarly, Kim's group has reported uncommon bending of long-chain alkanes in CB-[8] host molecules.[26,34] The much larger extent of coiling and structural distortion is energetically not favorable, as **4′** is ∼2 kcal/mol higher in energy at 3.1 kcal/mol than **4**. Thus, it is true that the linear arrangement that brings the terminal C−H bond closer to the superoxo moiety is more favorable, but the CB-[6] host offers enough space for the recoiling motion to take place, which gives access to the lower energy transition state **4′-TS**. We believe that such recoiling can activate the secondary C−H bond better compared to its primary analog. Our optimized structures of **4** and **4′** in Figure 5 clearly reveal a small but significant elongation of secondary C−H bond that can enable HAT through the superoxo radical in near proximity.

CONCLUSIONS

In summary, we propose an unprecedented vanadium-superoxo intermediate inside the CB-[6] host to be the catalytically active species. Our study reveals several insights of C−H activation carried out by the supramolecular catalyst. Based on extensive DFT calculations, the role of CB-[6] is revealed to be multifaced. First, CB-[6] acts as a ligand that binds the vanadyl ion. Next, the host stabilizes the superoxo radical through hydrophobic interactions. Finally, the CB-[6] portal oxygens dictate the regioselectivity of unactivated C−H bonds. We propose that unstable dioxygen intermediates can be trapped within the host whose half-life can be enhanced considerably. These adducts can enable C−H activation with excellent chemo- and regioselectivity through favorable host−guest interactions. Our study highlights how the CB-[6] and vanadyl moieties work in concert to achieve efficient and selective C−H bond oxidation catalysis. Studies toward exploiting these insights to develop other supramolecular catalysts are currently underway in our laboratory.

EXPERIMENTAL SECTION

All electronic structure calculations were carried out using DFT[35] as implemented in the Jaguar 9.1 suite[36] of ab initio quantum chemistry programs. Dispersion-corrected geometry optimizations were conducted with the B3LYP[37−41] functional including Grimme's D3 dispersion correction[42] and the 6-31G** basis set. Vanadium was represented using the Los Alamos LACVP** basis[43,44] that includes effective core potentials. The energies of the optimized structures were reevaluated with a larger basis set using the same functional and Dunning's correlation consistent triple-ζ basis set cc-pVTZ(-f)[45] which includes a double set of polarization functions. A modified version of LACVP has been employed for vanadium, designated as LACV3P, in which the exponents were decontracted to match the effective core potential with triple-ζ quality. A self-consistent reaction field (SCRF)[46−48] approach based on accurate numerical solutions of the Poisson−Boltzmann equation was employed for solvation energies. In the results reported, solvation calculations were performed with the 6-31G**/LACVP basis at the optimized gas phase geometry using the dielectric constant of ε = 35.6 for acetonitrile. Analytical vibrational frequencies within the harmonic approximation were computed with the 6-31G**/LACVP basis to

DOI: 10.1021/acs.inorgchem.9b02803
Inorg. Chem. 2019, 58, 16250−16255

confirm proper convergence to well-defined minima or saddle points on the potential energy surface.

The energy components have been computed with the following protocol. The free energy in solution phase $G(\mathrm{sol})$ has been calculated as follows:

$$G(\mathrm{sol}) = G(\mathrm{gas}) + G^{\mathrm{solv}} \quad (2)$$

$$G(\mathrm{gas}) = H(\mathrm{gas}) - TS(\mathrm{gas}) \quad (3)$$

$$H(\mathrm{gas}) = E(\mathrm{SCF}) + \mathrm{ZPE} \quad (4)$$

$$\Delta E(\mathrm{SCF}) = \sum E(\mathrm{SCF})\ \text{for products} - \sum E(\mathrm{SCF})\ \text{for reactants} \quad (5)$$

$$\Delta G(\mathrm{sol}) = \sum G(\mathrm{sol})\ \text{for products} - \sum G(\mathrm{sol})\ \text{for reactants} \quad (6)$$

where $G(\mathrm{gas})$ is the free energy in the gas phase; G^{solv} is the free energy of solvation as computed using the continuum solvation model; $H(\mathrm{gas})$ is the enthalpy in the gas phase; T is the temperature (298.15 K); $S(\mathrm{gas})$ is the entropy in the gas phase; $E(\mathrm{SCF})$ is the self-consistent field energy, i.e., "raw" electronic energy as computed from the SCF procedure, and ZPE is the zero point energy. Note that by entropy here we refer specifically to the vibrational/rotational/translational entropy of the solute(s); the entropy of the solvent is incorporated implicitly in the continuum solvation model.

EPR calculations are carried out with ORCA 4.0.1.[49] The ground state and excited state electronic structures of **1** and **2** are elucidated using the parameters derived from EPR and d-d transitions. These parameters are computed with the coupled perturbed (CP)-DFT-based method derived from B3LYP density functional. Here, a CP(PPP) (V),[50,51] EPR-II[52] (N of coordinated en_2 ligand) basis sets are used, while the remaining atoms were treated with the def2-SV(P) basis set.[53] ^{51}V hyperfine coupling constants were calculated with the spin−orbit contributions. The importance of relativistic effects are accounted using ZORA.

■ ASSOCIATED CONTENT

Supporting Information

The Supporting Information is available free of charge on the ACS Publications website at DOI: 10.1021/acs.inorgchem.9b02803.

Different binding modes of vanadyl binding to CB-[6]; (Figures S1−S3) electrostatic plots and optimized transition states; (Table S1) DFT-optimized structures energy components; and Cartesian coordinates of the optimized geometries (PDF)

■ AUTHOR INFORMATION

Corresponding Author

*E-mail: mbaik2805@kaist.ac.kr.

ORCID

Mahesh Sundararajan: 0000-0002-1522-124X

Bohyun Park: 0000-0003-0552-8763

Mu-Hyun Baik: 0000-0002-8832-8187

Notes

The authors declare no competing financial interest.

■ ACKNOWLEDGMENTS

We thank the Institute for Basic Science (computational studies, IBS-R010-A1) in South Korea for financial support. M.S. thanks DAE for sanctioning EOL.

■ REFERENCES

(1) Karlin, K. D. Metalloenzymes, Structural Motifs, and Inorganic Models. *Science* **1993**, *261* (5122), 701−708.

(2) Nam, W.; Lee, Y.-M.; Fukuzumi, S. Hydrogen Atom Transfer Reactions of Mononuclear Nonheme Metal-Oxygen Intermediates. *Acc. Chem. Res.* **2018**, *51* (9), 2014−2022.

(3) Feng, Z.; Zhang, T.; Wang, H.; Xu, B. Supramolecular Catalysis and Dynamic Assemblies for Medicine. *Chem. Soc. Rev.* **2017**, *46* (21), 6470−6479.

(4) Meeuwissen, J.; Reek, J. N. H. Supramolecular Catalysis beyond Enzyme Mimics. *Nat. Chem.* **2010**, *2* (8), 615−621.

(5) Lagona, J.; Mukhopadhyay, P.; Chakrabarti, S.; Isaacs, L. The Cucurbit[n]uril Family. *Angew. Chem., Int. Ed.* **2005**, *44* (31), 4844−4870.

(6) Lee, J. W.; Samal, S.; Selvapalam, N.; Kim, H.-J.; Kim, K. Cucurbituril Homologues and Derivatives: New Opportunities in Supramolecular Chemistry. *Acc. Chem. Res.* **2003**, *36* (8), 621−630.

(7) Barrow, S. J.; Kasera, S.; Rowland, M. J.; del Barrio, J.; Scherman, O. A. Cucurbituril-Based Molecular Recognition. *Chem. Rev.* **2015**, *115* (22), 12320−12406.

(8) de Lima, S. M.; Gómez, J. A.; Barros, V. P.; Vertuan, G. de S.; Assis, M. D.; Graeff, C. F. O.; Demets, G. J.-F. A New oxovanadium(IV)−cucurbit[6]uril Complex: Properties and Potential for Confined Heterogeneous Catalytic Oxidation Reactions. *Polyhedron* **2010**, *29* (15), 3008−3013.

(9) Langeslay, R. R.; Kaphan, D. M.; Marshall, C. L.; Stair, P. C.; Sattelberger, A. P.; Delferro, M. Catalytic Applications of Vanadium: A Mechanistic Perspective. *Chem. Rev.* **2019**, *119* (4), 2128−2191.

(10) Schwendt, P.; Sivák, M. Composition and Structure of Vanadium(V) Peroxo Complexes. *Vanadium Compounds* **1998**, *711*, 117−125.

(11) Butler, A.; Clague, M. J.; Meister, G. E. Vanadium Peroxide Complexes. *Chem. Rev.* **1994**, *94* (3), 625−638.

(12) Waidmann, C. R.; DiPasquale, A. G.; Mayer, J. M. Synthesis and Reactivity of Oxo-Peroxo-vanadium(V) Bipyridine Compounds. *Inorg. Chem.* **2010**, *49* (5), 2383−2391.

(13) Comba, P.; Kuwata, S.; Linti, G.; Tarnai, M.; Wadepohl, H. Synthesis and Oxidation of Vanadyl Complexes Containing Bispidine Ligands. *Eur. J. Inorg. Chem.* **2007**, *2007* (5), 657−664.

(14) Gekhman, A. E.; Stolarov, I. P.; Moiseeva, N. I.; Rubaijlo, V. L.; Vargaftik, M. N.; Moiseev, I. I. Oxidations in the H2O2VvAcOH System. Evidence of Vanadium (V) Complexes with Superoxide Anion and Singlet Dioxygen Molecule as Ligands. *Inorg. Chim. Acta* **1998**, *275*−*276*, 453−461.

(15) Shetti, V. N.; Rani, M. J.; Srinivas, D.; Ratnasamy, P. Chemoselective Alkane Oxidation by Superoxo-vanadium(V) in Vanadosilicate Molecular Sieves. *J. Phys. Chem. B* **2006**, *110* (2), 677−679.

(16) Zhang, J.; Yang, H.; Sun, T.; Chen, Z.; Yin, G. Nonredox Metal-Ions-Enhanced Dioxygen Activation by Oxidovanadium(IV) Complexes toward Hydrogen Atom Abstraction. *Inorg. Chem.* **2017**, *56* (2), 834−844.

(17) Kelm, H.; Krüger, H.-J. A Superoxovanadium(V) Complex Linking the Peroxide and Dioxygen Chemistry of Vanadium. *Angew. Chem., Int. Ed.* **2001**, *40* (12), 2344−2348.

(18) Hudzik, J. M.; Bozzelli, J. W.; Simmie, J. M. Thermochemistry of C7H16 to C10H22 Alkane Isomers: Primary, Secondary, and Tertiary C-H Bond Dissociation Energies and Effects of Branching. *J. Phys. Chem. A* **2014**, *118* (40), 9364−9379.

(19) Tian, Z.; Fattahi, A.; Lis, L.; Kass, S. R. Cycloalkane and Cycloalkene C−H Bond Dissociation Energies. *J. Am. Chem. Soc.* **2006**, *128* (51), 17087−17092.

(20) Ballhausen, C. J.; Gray, H. B. The Electronic Structure of the Vanadyl Ion. *Inorg. Chem.* **1962**, *1* (1), 111−122.

(21) Nam, W. Synthetic Mononuclear Nonheme Iron-Oxygen Intermediates. *Acc. Chem. Res.* **2015**, *48* (8), 2415−2423.

(22) Holland, P. L. Metal-Dioxygen and Metal-Dinitrogen Complexes: Where Are the Electrons? *Dalton Trans.* **2010**, *39* (23), 5415−5425.

DOI: 10.1021/acs.inorgchem.9b02803
Inorg. Chem. 2019, 58, 16250−16255

(23) Bardelang, D.; Banaszak, K.; Karoui, H.; Rockenbauer, A.; Waite, M.; Udachin, K.; Ripmeester, J. A.; Ratcliffe, C. I.; Ouari, O.; Tordo, P. Probing Cucurbituril Assemblies in Water with TEMPO-like Nitroxides: A Trinitroxide Supraradical with Spin-Spin Interactions. *J. Am. Chem. Soc.* **2009**, *131* (15), 5402−5404.
(24) Sundararajan, M.; Solomon, R. V.; Ghosh, S. K.; Venuvanalingam, P. Elucidating the Structures and Binding of Halide Ions Bound to cucurbit[6]uril, Hemi-cucurbit[6]uril and bambus[6]-uril Using DFT Calculations. *RSC Adv.* **2011**, *1* (7), 1333−1341.
(25) Florea, M.; Nau, W. M. Strong Binding of Hydrocarbons to Cucurbituril Probed by Fluorescent Dye Displacement: A Supramolecular Gas-Sensing Ensemble. *Angew. Chem., Int. Ed.* **2011**, *50* (40), 9338−9342.
(26) Sundararajan, M. Quantum Chemical Challenges for the Binding of Simple Alkanes to Supramolecular Hosts. *J. Phys. Chem. B* **2013**, *117* (43), 13409−13417.
(27) Meunier, B.; de Visser, S. P.; Shaik, S. Mechanism of Oxidation Reactions Catalyzed by Cytochrome p450 Enzymes. *Chem. Rev.* **2004**, *104* (9), 3947−3980.
(28) Baik, M.-H.; Newcomb, M.; Friesner, R. A.; Lippard, S. J. Mechanistic Studies on the Hydroxylation of Methane by Methane Monooxygenase. *Chem. Rev.* **2003**, *103* (6), 2385−2419.
(29) (a) Green, A. G.; Liu, P.; Merlic, C. A.; Houk, K. N. Distortion/Interaction Analysis Reveals the Origins of Selectivities in Iridium-Catalyzed C−H Borylation of Substituted Arenes and 5-Membered Heterocycles. *J. Am. Chem. Soc.* **2014**, *136* (12), 4575−4583. (b) Bickelhaupt, F. M.; Houk, K. N. Analyzing Reaction Rates with the Distortion/Interaction-Activation Strain Model. *Angew. Chem., Int. Ed.* **2017**, *56*, 10070−10086.
(30) Freeman, W. A.; Mock, W. L.; Shih, N. Y. Cucurbituril. *J. Am. Chem. Soc.* **1981**, *103* (24), 7367−7368.
(31) Vallavoju, N.; Sivaguru, J. Supramolecular Photocatalysis: Combining Confinement and Non-Covalent Interactions to Control Light Initiated Reactions. *Chem. Soc. Rev.* **2014**, *43* (12), 4084−4101.
(32) Isaacs, L. Stimuli Responsive Systems Constructed Using Cucurbit[n]uril-Type Molecular Containers. *Acc. Chem. Res.* **2014**, *47* (7), 2052−2062.
(33) Ajami, D.; Rebek, J., Jr. More Chemistry in Small Spaces. *Acc. Chem. Res.* **2013**, *46* (4), 990−999.
(34) Baek, K.; Kim, Y.; Kim, H.; Yoon, M.; Hwang, I.; Ko, Y. H.; Kim, K. Unconventional U-Shaped Conformation of a Bolaamphiphile Embedded in a Synthetic Host. *Chem. Commun.* **2010**, *46* (23), 4091−4093.
(35) Calais, J.-L. Density-Functional Theory of Atoms and Molecules. *Int. J. Quantum Chem.* **1993**, *47* (1), 101−101.
(36) Bochevarov, A. D.; Harder, E.; Hughes, T. F.; Greenwood, J. R.; Braden, D. A.; Philipp, D. M.; Rinaldo, D.; Halls, M. D.; Zhang, J.; Friesner, R. A. Jaguar: A High-Performance Quantum Chemistry Software Program with Strengths in Life and Materials Sciences. *Int. J. Quantum Chem.* **2013**, *113* (18), 2110−2142.
(37) Slater, J. C.; Phillips, J. C. Quantum Theory of Molecules and Solids Vol. 4: The Self-Consistent Field for Molecules and Solids. *Phys. Today* **1974**, *27*, 49−50.
(38) Vosko, S. H.; Wilk, L.; Nusair, M. Accurate Spin-Dependent Electron Liquid Correlation Energies for Local Spin Density Calculations: A Critical Analysis. *Can. J. Phys.* **1980**, *58* (8), 1200−1211.
(39) Becke, A. D. Density-Functional Exchange-Energy Approximation with Correct Asymptotic Behavior. *Phys. Rev. A: At., Mol., Opt. Phys.* **1988**, *38* (6), 3098−3100.
(40) Becke, A. D. Density-functional Thermochemistry. III. The Role of Exact Exchange. *J. Chem. Phys.* **1993**, *98* (7), 5648−5652.
(41) Lee, C.; Yang, W.; Parr, R. G. Development of the Colle-Salvetti Correlation-Energy Formula into a Functional of the Electron Density. *Phys. Rev. B: Condens. Matter Mater. Phys.* **1988**, *37* (2), 785−789.
(42) Grimme, S.; Antony, J.; Ehrlich, S.; Krieg, H. A Consistent and Accurate Ab Initio Parametrization of Density Functional Dispersion Correction (DFT-D) for the 94 Elements H-Pu. *J. Chem. Phys.* **2010**, *132* (15), 154104.
(43) Hay, P. J.; Wadt, W. R. Ab Initio Effective Core Potentials for Molecular Calculations. Potentials for the Transition Metal Atoms Sc to Hg. *J. Chem. Phys.* **1985**, *82* (1), 270−283.
(44) Hay, P. J.; Wadt, W. R. Ab Initio Effective Core Potentials for Molecular Calculations. Potentials for K to Au Including the Outermost Core Orbitals. *J. Chem. Phys.* **1985**, *82* (1), 299−310.
(45) Dunning, T. H. Gaussian Basis Sets for Use in Correlated Molecular Calculations. I. The Atoms Boron through Neon and Hydrogen. *J. Chem. Phys.* **1989**, *90* (2), 1007−1023.
(46) Marten, B.; Kim, K.; Cortis, C.; Friesner, R. A.; Murphy, R. B.; Ringnalda, M. N.; Sitkoff, D.; Honig, B. New Model for Calculation of Solvation Free Energies: Correction of Self-Consistent Reaction Field Continuum Dielectric Theory for Short-Range Hydrogen-Bonding Effects. *J. Phys. Chem.* **1996**, *100* (28), 11775−11788.
(47) Friedrichs, M.; Zhou, R.; Edinger, S. R.; Friesner, R. A. Poisson−Boltzmann Analytical Gradients for Molecular Modeling Calculations. *J. Phys. Chem. B* **1999**, *103*, 3057−3061.
(48) Edinger, S. R.; Cortis, C.; Shenkin, P. S.; Friesner, R. A. Solvation Free Energies of Peptides: Comparison of Approximate Continuum Solvation Models with Accurate Solution of the Poisson−Boltzmann Equation. *J. Phys. Chem. B* **1997**, *101*, 1190−1197.
(49) Neese, F. Software Update: The ORCA Program System, Version 4.0. *WIREs Comput. Mol. Sci.* **2018**, *8* (1), e1327.
(50) Neese, F. Prediction and Interpretation of the 57Fe Isomer Shift in Mössbauer Spectra by Density Functional Theory. *Inorg. Chim. Acta* **2002**, *337*, 181−192.
(51) Sinnecker, S.; Slep, L. D.; Bill, E.; Neese, F. Performance of Nonrelativistic and Quasi-Relativistic Hybrid DFT for the Prediction of Electric and Magnetic Hyperfine Parameters in ^{57}Fe Mössbauer Spectra. *Inorg. Chem.* **2005**, *44* (7), 2245−2254.
(52) Barone, V.; Bencini, A.; Fantucci, P. *Recent Advances In Density Functional Methods* **2002**, *1*, 1.
(53) Schäfer, A.; Horn, H.; Ahlrichs, R. Fully Optimized Contracted Gaussian Basis Sets for Atoms Li to Kr. *J. Chem. Phys.* **1992**, *97* (4), 2571−2577.

DOI: 10.1021/acs.inorgchem.9b02803
Inorg. Chem. 2019, 58, 16250−16255